J. Phys. D: Appl. Phys. **31** (1998) 663–670. Printed in the UK PII: S0022-3727(98)86420-6

The correlation between mechanical stress and magnetic properties of ultrathin films

D Sander, R Skomski, A Enders, C Schmidthals, D Reuter and J Kirschner

Max-Planck-Institut für Mikrostrukturphysik, Weinberg 2, D-06120 Halle, Germany

Received 24 July 1997

Abstract. The cantilever bending beam technique was applied to measure film stress, film magnetization and magneto-elastic coupling in nanometre Fe films grown epitaxially on W substrates. A simple optical deflection technique yielded sub-monolayer sensitivity for stress measurements and was used to determine magnetization and magnetostrictive properties of nanometre Fe films *in situ*. The combination of an electromagnet inside an ultra-high-vacuum chamber with a rotatable external magnet was employed to perform magneto-optical Kerr-effect measurements in the transversal, longitudinal and polar geometry in fields of up to 0.4 T. Examples for stress-driven structural changes in monolayer Fe films are discussed with respect to the unusual high coercivity found for sesquilayer Fe films and the re-orientation of the easy axis of magnetization in Stranski–Krastanov Fe films. The direct correlation between strain and magnetism was exploited to measure the magnetostrictive bending of the film–substrate composite. The magnitude and sign of the magneto-elastic coupling coefficient were found to depend on the film thickness, in contrast to the respective bulk values.

1. Introduction

The experimental and theoretical study of the unique magnetic properties of ultrathin ferromagnetic films with thicknesses of the order of nanometres has attracted considerable attention in recent review articles [1–3] and books [4]. One fundamental aspect of the hetero-epitaxial growth is how the lattice mismatch between film and substrate induces characteristic changes in the structural and magnetic properties of the ferromagnetic film. Owing to the often very strong bond between the film material and the substrate of up to 5 eV per film atom, as has been determined for example by thermal desorption experiments [5], the first monolayer of the growing film remains pseudomorphic in registry with the substrate even in cases in which the lattice mismatch between the bulk atomic distances of the film material and the substrate reaches values of 10% and more. Examples for such heavily strained monolayers are the growth of Fe, Co and Ni on W(110). Structural investigations by low-energy electron diffraction (LEED) [6] and scanning tunnelling microscopy (STM) [7] proved that the first monolayer of Fe on W(110) remains pseudomorphic, thus heavily strained (by 9.4%). The even larger lattice mismatch of 27% for the growth of Ni on W(110) does not hinder pseudomorphic growth in the sub-monolayer range, as was found in LEED [8] and combined STM and LEED studies [9]. Without going into details of the elasticity theory applied to epitaxial growth [10], a crude estimate with a typical Young modulus of order 10^{11} N m^{-2} gives a tremendous film stress of order 1 GPa (1000 N mm^{-2}) per 1% lattice mismatch. Film stress of that order is expected to modify the growth of hetero-epitaxial films considerably, due to the tremendous elasticity energy of order 0.1 eV per atom in a film strained by only 1%. Therefore, film stress is expected to be a dominant driving force for structural transitions in ultrathin Fe films on W(110) and will be discussed in this paper. The formation of a misfit distortion network for room temperature growth or the island formation observed for Stranski–Krastanov growth at higher temperatures are ascribed to a reduction of film stress that was measured *in situ* with sub-monolayer sensitivity. The effect of film stress and its relaxation on the coercivity and the easy axis of magnetization are examined *in situ* with the magneto-optical Kerr-effect (MOKE). A most direct manifestation of the intimate relation between the strain state and magnetism came from magnetostriction experiments that were performed to investigate the magneto-elastic coupling in nanometre Fe films on W(100).

In the following experimental section, the basic idea of our stress-measurement set-up is described and the lay-out of the magnetic system to perform MOKE and magnetostriction experiments is given. Then, the stress and magnetic properties of Fe films grown at room temperature in the Frank–van der Merwe mode are discussed, before the effects of island formation in Stranski–Krastanov

0022-3727/98/060663+08$19.50

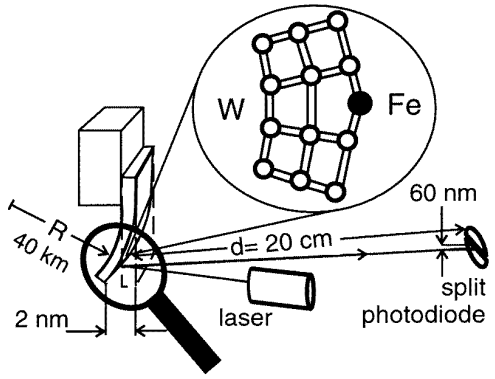

Figure 1. A schematic diagram of the optical deflection technique. Any stress on the front surface of the crystal induces a minute bending, characterized by the radius of curvature *R*, that is detected by reflecting a laser beam from the bottom end of the crystal to a position-sensitive detector. The image shows the compressive stress; the numbers correspond to the sensitivity limits. The laser and a split photodiode are mounted onto an UHV window flange [17].

Fe layers grown at higher temperatures on stress and magnetism are presented. The application of the stress-measurement technique to determine film magnetization and magnetostriction concludes this paper.

2. The stress-measurement technique

In order to measure film stress with monolayer sensitivity during growth, the cantilever bending beam technique was employed. As shown in the schematic diagram of our optical deflection technique in figure 1, the main idea of the film-stress measurement was to monitor the bending of a substrate due to any kind of adsorption processes on its front surface, whereas the back side of the substrate remained clean. Any change of the stress state of the front surface of the substrate will lead to a minute bending. Thus, monitoring the change of the radius of curvature of the substrate allows one to determine the change of the stress on the front surface. From a measurement of the radius of curvature R the stress τ in units of force per length can be calculated from Stoney's formula [11] that is corrected by the factor $1/(1-\nu)$ to take the biaxial nature of the stress into account:

$$\tau = \frac{Yt^2}{6R(1-\nu)}.$$

To get sub-monolayer sensitivity, rather thin substrates with thicknesses t of order 0.1 mm have to be used. Young's modulus Y and the Poisson ratio ν of the substrate have to be calculated for the particular substrate surface orientation [12]. The applicability of Stoney's equation to measure epitaxial stress [13] and magnetostrictive stress [14] has been discussed by Marcus. Capacitive [15] and optical techniques [16] have been employed to measure stress with sub-monolayer sensitivity. In capacitive techniques, the change in distance between the bottom end of the substrate and a fixed reference electrode is determined from the change in capacity and translated into a radius of curvature. In optical techniques, a light beam is reflected from the bottom end of the substrate onto a position-sensitive detector. The bending of the substrate causes a deflection of the beam that is measured as a position signal and converted into a stress value. As we have described in detail elsewhere [17], our simple and compact optical deflection technique sketched in figure 1 can be mated to any UHV viewport and allows us to detect a radius of curvature as large as 40 km, which corresponds to a deflection of the bottom end of the approximately 10 mm long sample by only 2 nm, giving sub-monolayer sensitivity. On the position-sensitive detector, an easily measurable deflection of almost 0.1 μm results. The high sensitivity allows one to measure not only film stress, but also adsorbate-induced stress [18] and forces in ferromagnetic films due to the torque of a magnetized film in an external field and due to magnetostriction in the ferromagnetic layer. The combined application of the cantilever technique to measure stress, film magnetization and magnetostriction has been demonstrated before with a capacitive technique [19]. We employ the somewhat simpler optical deflection technique that gives a comparable sensitivity. Note that magnetostrictive strains of order 10^{-5} are three orders of magnitude smaller than misfit strains in the 1% range. Thus, for detecting magnetostriction of a monolayer film, the sensitivity has to be 1000 times higher than that for measurement of the stress of a monolayer film! Currently, the detection limit for magnetostriction both of capacitive and of optical techniques is of the order of ten monolayers of Fe [20].

3. Transversal, longitudinal and polar magnetic fields

To correlate the stress and magnetism of ultrathin films *in situ*, we incorporated two magnets into our ultra-high vacuum (UHV) chamber. As shown in the schematic cross section of a part of our UHV chamber in figure 2, the sample (1) can be exposed to a magnetic field of up to 0.1 T along its length by a pair of water-cooled electromagnets (2). In position (1), Kerr-effect measurements [21] in the transversal geometry (A) are performed. Lowering the sample to position (3) allows one to measure the longitudinal Kerr effect (B) with an external electromagnet (4). Its pole pieces (5) are mounted inside the UHV chamber on a turntable and direct the magnetic field to the sample. The external magnet and the pole pieces (5) are mounted on two separate turntables; thus, without having to rearrange the Kerr-optics, the magnetic field can be oriented perpendicular to the sample surface for polar Kerr-effect measurements. Longitudinal and polar Kerr-measurements are performed in fields of up to 0.4 T. With the sample in the lower position (3), the vertical magnetic field produced by the water-cooled electromagnet (2) gives a vertical field component of up to 0.03 T. Thus, at position (3), magnetic fields with arbitrary direction can be produced by vector addition of the respective field components. At position (3) the optical stress-measurement set-up is mounted onto an UHV window to perform magnetometry and magnetostriction experiments.

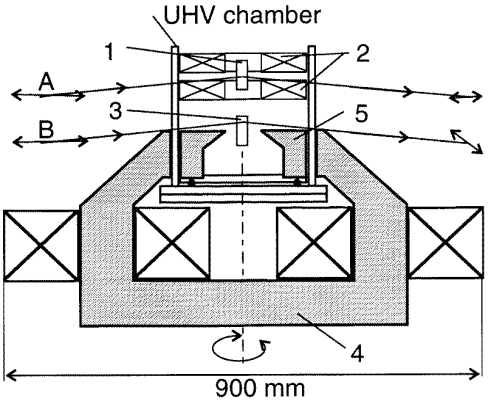

Figure 2. A cross section through the lower part of the UHV chamber. The sample in position (1) can be exposed to a vertical magnetic field produced by the water-cooled electromagnet (2) that is mounted inside the UHV chamber. At position (3), the sample can be exposed to a horizontal and polar magnetic field produced by the external electromagnet (4) with pole pieces (5). Magnet (4) and pole pieces (5) are rotatable, allowing in-plane and out-of-plane magnetization. Transversal Kerr measurements (A) are performed in fields of up to 0.1 T; longitudinal and polar Kerr measurements (B) are possible in fields of up to 0.4 T.

For magnetometry, the film is first magnetized along its length by magnet (1) and then exposed to a polar magnetic field, produced by the external magnet (4), rotated to the polar position. Thus a torque is acting on the film that leads to a bending of the substrate. As indicated in figure 7 later and discussed below, from the measured bending of the sample the film magnetization is determined. To measure magnetostriction, the magnetization is switched between the horizontal and vertical directions by applying fields of the external magnet (4) and the UHV magnet (2) and the corresponding magnetostrictive bending of the sample is detected. Simultaneously, Kerr-effect measurements are performed to identify the appropriate magnetization states, as shown in figure 8 later.

4. Stress and stress relaxation in Fe monolayers on W(110)

The growth of Fe on W is governed by the large lattice mismatch of almost 10% between Fe and W. A number of previous structural investigations by LEED [6] and STM [7] revealed a pseudomorphic first Fe monolayer on W(110). One monolayer (ML) is defined as 1.41×10^{15} Fe atoms per cm^2, equivalent to a monolayer thickness of 1.66 Å. From the expression for the elastic energy density of a BCC (110) surface, the resulting stress in the strained Fe film can be calculated. The first layer of Fe grows heavily strained by almost 10%, and a huge anisotropic *tensile* film stress of order 5.6 N m^{-1} per monolayer along W[001] and of 7.9 N m^{-1} per monolayer along W[$\bar{1}$10] is predicted from the application of continuum elasticity, based on bulk reference data. The stress anisotropy simply reflects the only two-fold rotational symmetry of the BCC (110) surface. In striking contrast to the results of continuum elasticity, we measure *compressive* stress for sub-monolayer coverages of Fe on W(110), as shown in our stress curves of figure 3. The maximum compressive stress is reached at approximately 0.6 ML and amounts to a tremendous -5 N m^{-1} for room-temperature growth and -3 N m^{-1} for high-temperature growth, as shown in figures 3(a) and (c), respectively. These results indicate that the pseudomorphic Fe islands at a coverage of 0.6 ML induce a huge compressive stress of order 35 GPa on the W surface. As has been discussed in more detail elsewhere [22], we ascribe the compressive sub-monolayer stress to a mere surface stress effect, indicating the inappropriateness of continuum elasticity based on bulk reference data for application to the sub-monolayer range. Only for coverages above 0.6 ML does the continuum elasticity describe the film stress at least qualitatively, as manifested by our finding of a tensile film stress of order 6 N m^{-1} per monolayer, estimated from the slopes of the stress curves in the coverage range 0.7–1.5 ML. The stress measurements revealed a distinct kink in the slope of the stress versus coverage curve at a coverage of 1.5 ML (2.5 Å) Fe. Whereas the slope of the curve was reduced from 6 to 3 N m^{-1} per monolayer for the room-temperature growth shown in figure 3(a), deposition at 700 K (figure 3(b)) led to an even more pronounced reduction to 1 N m^{-1}. Deposition at 1000 K (figure 3(c)) led to practically stress-free growth after the kink at 1.5 ML. For room-temperature growth, no stress relaxation was observed after termination of growth, whereas deposition at higher temperatures led to a partial stress relaxation after growth, the relaxation being strongest for high-temperature growth at 1000 K. Here, the stress of a 12 Å (7 ML) thick Fe film relaxed to 4 N m^{-1} compared with 15 N m^{-1} for room-temperature growth. The kink of the stress curves at the sesquilayer coverage of 1.5 ML was ascribed to the formation of a misfit distortion network in the Fe film. Owing to the high strain energy of the pseudomorphic phase, already at 1.5 ML coverage the formation of misfit distortions is triggered and relaxes part of the strain energy of the film. The contribution of the misfit distortions and the resulting inhomogeneous stress field to the high coercivity of the sesquilayer film is discussed in the following section. *In situ* LEED revealed a regular distortion pattern of a 3 ML Fe film, as indicated in figure 4(a) and described previously [6]. STM images of a 3 ML film in figure 3(b) identified a regular distortion line network in the Fe film as hexagonal shaped darker lines on the lighter grey Fe patches of the third and fourth layers. In accordance with a detailed STM analysis of the distortion pattern [7], we ascribe the kink of the stress curves at 1.5 ML to the onset of the formation of misfit distortions at the interface between the first and the second Fe layer. The first layer remains pseudomorphic, whereas already in the second layer the misfit distortions induce a partial relief of stress in the film, manifested by the reduced slope of the stress curves. This stress-relief mechanism due to the formation of misfit distortions is most efficient at high growth temperatures, which suggests that it is a thermally activated process. Growth at higher temperatures leads to the formation of Fe islands on top of the first Fe monolayer that covers the W surface pseudomorphically [23]. A double diffraction pattern with the lattice constants of BCC

(110) W and BCC (110) Fe, respectively, is observed in the LEED image of figure 4(c). The STM image of figure 4(d) identifies for a 3 nm Fe film grown at 300 K to 700 K, after annealing, islands elongated along W[001] with lengths of 10 μm, widths of 0.1 μm and maximum heights of 17 nm. The same diffraction and STM images were obtained upon annealing a room-temperature-grown film and for deposition at higher temperatures, indicating the equivalence of the two experimental procedures in producing Stranski–Krastanov Fe layers. Scanning Auger microscopy proved that, in between the islands, 1 ML of Fe covers the W surface [24]. As discussed in the following section on magnetism, the coalescence of Fe into 3D islands induces an in-plane re-orientation of the easy axis of magnetization in the Fe islands. The measured stress for high-temperature growth is ascribed to the first monolayer alone, whereas the formation of the 3D Fe islands does not increase the film stress any further, as indicated by the horizontal section of the stress curve measured during Fe deposition of figure 3(c). Some relaxation of stress after termination of growth leads to a final stress indicative of the strained first monolayer.

5. The high coercivity and re-orientation of the easy axis of magnetization

The most significant structural change for room-temperature-grown Fe films is the formation of a misfit distortion network at the sesquilayer coverage of 1.5 ML. Deposition of Fe at higher temperatures and annealing room-temperature-grown films to 700 K lead to the formation of 3D Fe islands, characteristic of Stranski–Krastanov growth. Both structural transitions, the formation of misfit distortions and the island formation, induce characteristic changes of the film magnetism, affecting the coercivity and the orientation of the easy axis of magnetization, respectively.

As discussed in more detail previously [22], the coercivity of Fe on W(110) shows a pronounced maximum at the sesquilayer coverage of 1.5 ML. The striking thickness dependence of the coercivity is clearly indicated by longitudinal Kerr-effect measurements on an Fe film with a mesa-shaped thickness variation, summarized in figure 5. The Fe film thickness was changed over the sample length by moving the crystal during evaporation in front of the Fe evaporator. The resulting thickness profile, which was checked with Auger electron spectroscopy, is given in figure 5(a): the thickness increased from 0.8 ML at one end of the crystal to 2 ML at the middle of the crystal and then dropped to 0.8 ML at the other end of the crystal, covering a total length of 8 mm. MOKE was performed with a collimated laser beam, thus by scanning the laser over the crystal length, different Fe thicknesses were probed *in situ*. Figure 5(b) shows two clear maxima of the coercivity of order 0.2 T for the slopes of the Fe film, for which the thickness was 1.5 ML. Note that the maximum is quite sharp on the thickness scale. The 0.8 ML film had a coercivity smaller than 0.02 T; the 2 ML film had a coercivity smaller than 0.07 T. Figure 5(c) shows results from a MOKE experiment performed on a single sesquilayer film in the longitudinal geometry. Here, the

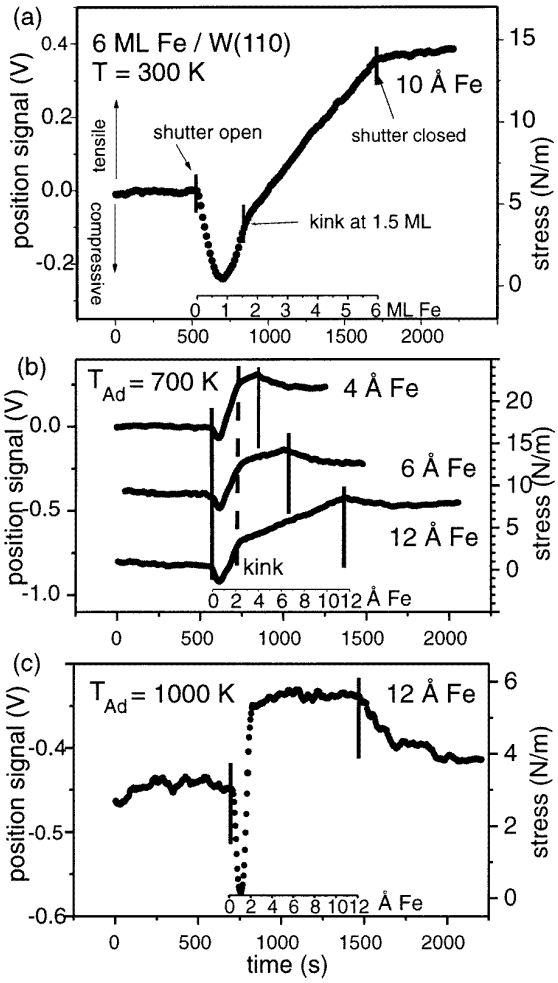

Figure 3. Stress measurements during Fe growth on W(110). (a) The growth of 6 ML Fe at 300 K. The kink indicates the formation of the misfit distortion network. (b) The growth of several thicknesses at 700 K. A partial relief of stress after termination of growth is visible; the kink remains at 1.5 ML coverage. (c) The growth of 12 Å at 1000 K. Note the stress-free growth after the kink at 1.5 ML.

coercivity was higher than 0.3 T at 140 K; only at the slightly higher temperature of 190 K could the film be magnetized with a coercivity of 0.2 T. A characteristic film structure in the sesquilayer range is presented in the STM image of figure 5(d). Lighter grey patches of the second layer of Fe were imaged on the darker grey first monolayer of Fe that covered the W surface homogeneously. The second-layer patches were of order 10–20 nm long and 5–10 nm wide. In the process of magnetization, a domain wall has to move in the sesquilayer film and its energy will depend on the local layer thickness, being either one monolayer or two monolayers in the second-layer patch. A simple estimate shows that the domain wall energy is higher for the two-layer region. Thus a pinning mechanism results that gives a maximum coercivity of order 0.6 T [22]. The contribution of the inhomogeneous stress field to the coercivity [25], once misfit distortions have been formed, can be estimated to be of order 0.07 T, suggesting that the

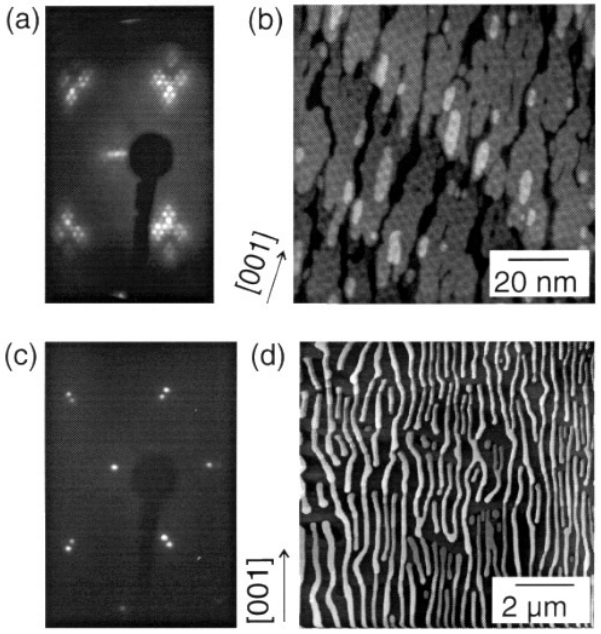

Figure 4. LEED and STM of Fe on W(110). (a) 3 ML Fe, grown at 300 K. The diffraction pattern of the distortion network to be seen in the STM image (b). A hexagonally shaped distortion line network appears as darker grey lines on the surface of the third (grey) and fourth (white) Fe layers. The underlying second Fe layer appears black. (c) Annealing to 700 K changes (a) to a double BCC (110) diffraction pattern, indicating W lattice distances and relaxed Fe distances. (d) A STM image of 3 nm Fe annealed to 700 K. Fe islands elongated in W[001] are seen as grey stripes; the maximum height is 17 nm.

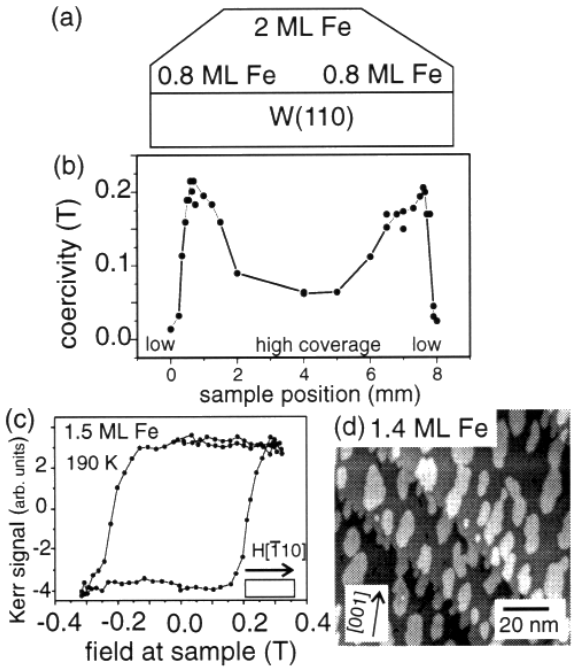

Figure 5. MOKE in the sesquilayer range. (a) A cross section of the mesa-shaped thickness variation of the Fe film. (b) Spatially resolved coercivities of film (a), measured at 140 K. Note two pronounced maxima where the thicknesses cross 1.5 ML. (c) Longitudinal MOKE on a sesquilayer film with constant thickness at 190 K. (d) A STM image of the sesquilayer film: islands of the second layer Fe appear as grey patches on the darker grey first monolayer Fe. Mono-atomic steps of the substrate appear as lines running from the upper left-hand side down to the lower right-hand side of the image.

thickness dependence of the domain wall energy is the main factor affecting the coercivity mechanism [22].

The formation of 3D Fe islands upon annealing a room-temperature-grown film induces a re-orientation of the easy axis of magnetization, as indicated by the MOKE curves of figure 6, that have partially been discussed elsewhere [26]. Rectangular transversal Kerr-effect curves indicate that there is an easy axis of magnetization along W[$\bar{1}$10] and a hard-axis curve in the longitudinal Kerr geometry for magnetization along W[001] for room-temperature growth of 10 ML Fe. Whereas fields of 0.25 T were sufficient to saturate the in-plane magnetization along the hard direction, polar magnetization did not lead to saturation. The continuous slope of the curve of the polar Kerr effect suggests that the effective anisotropy against out-of-plane magnetization, is even stronger than in-plane anisotropy, in accordance with previous work [27]. The pronounced in-plane anisotropy has been found to be thickness dependent. Fe(110) layers grown on GaAs and on W(110) have an easy axis of magnetization along [$\bar{1}$10] for small thicknesses that switches in-plane to [001] at thicknesses of 5 nm [28] and 10 nm [29], respectively. We found that the in-plane re-orientation of the easy axis of magnetization occurs even for much smaller Fe thicknesses, after annealing room-temperature-grown films. As shown in the lower row of figure 6, after annealing a 1.7 nm thick film, the easy magnetization could be observed along [001], whereas the former rectangular magnetization curve measured in the transversal geometry has been replaced by a hard-axis curve. The effective anisotropy opposing polar magnetization was increased, as we deduced from the reduced slope of the magnetization curve of the polar geometry. Annealing led to a coalescence of Fe into 3D islands, as indicated in the STM image of figure 4(d). Thus, the nominal thickness in the islands is considerably increased and the easy axis of magnetization re-orients to [001], which is the easy direction of bulk Fe. We ascribe this re-orientation of the easy axis of magnetization to the diminished importance of surface anisotropies in the thick Fe islands that had been proposed to be the main reason for the pronounced in-plane anisotropy of Fe films that had not been annealed [27, 29].

6. Magnetometry and magnetostriction by cantilever bending techniques

Forces acting on ferromagnetic films in external magnetic fields and forces due to magnetostriction of ferromagnetic films cause a bending of the film–substrate composite that can be evaluated to give film magnetization or magnetostriction constants. Vibrating-sample magnetometry and force magnetometry rely on the detection of the minute

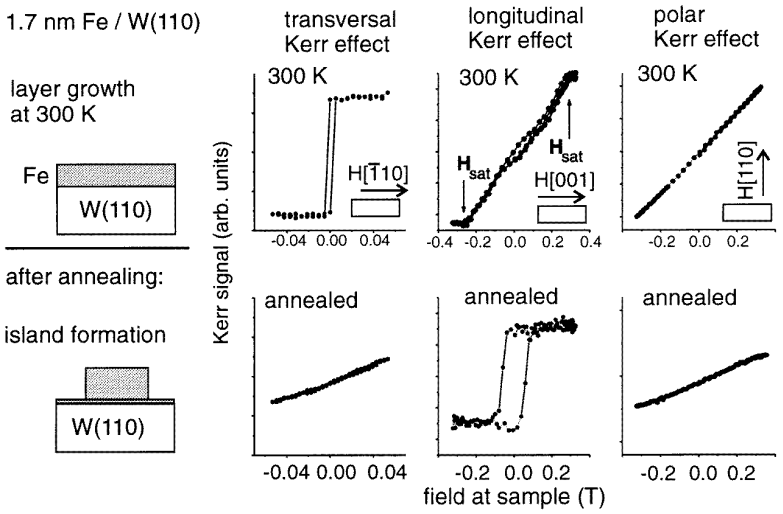

Figure 6. The effect of annealing on the direction of the easy axis of magnetization. The upper row shows MOKE on 1.7 nm, grown at 300 K. The easy axis is oriented along [1̄10]. The lower row is for the same film after annealing. The easy axis is re-oriented to [001].

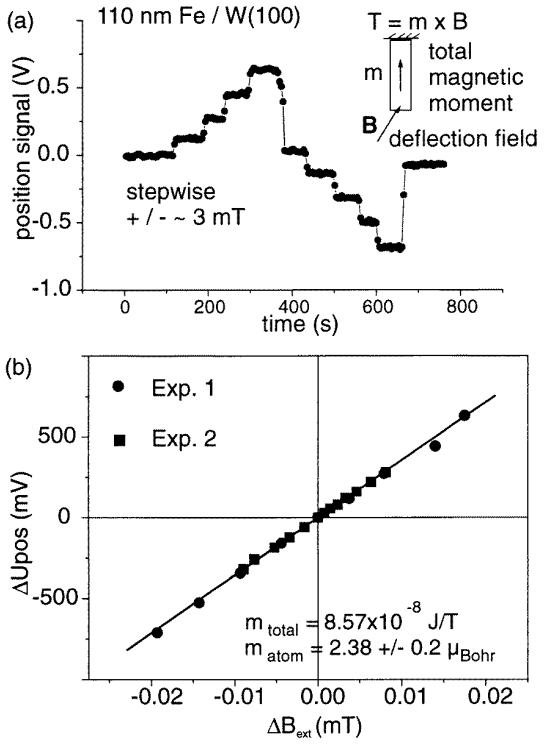

Figure 7. Magnetometry of 110 nm Fe on W(100). (a) A polar deflection field is increased stepwise and acts on the magnetized sample. A stepwise increasing torque T is induced and leads to a deflection of the sample that is detected by the change in the position signal. (b) The resulting deflection signal is proportional to the deflection field. The slope of the curve gives the total magnetic moment of the film.

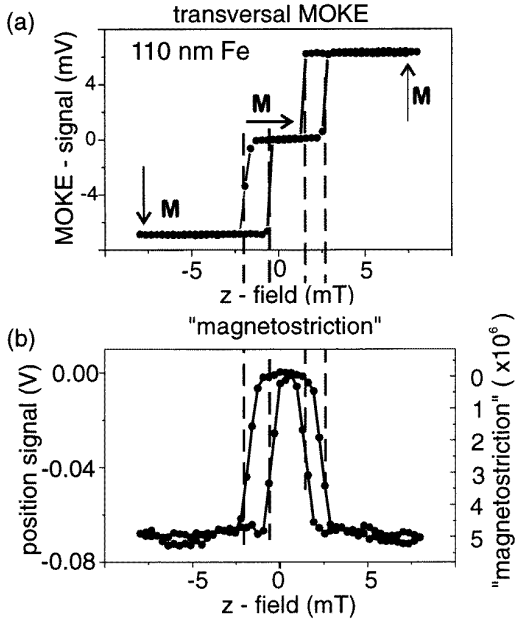

Figure 8. *In situ* MOKE and magnetostriction experiments with 110 nm Fe on W(100). (a) Transversal Kerr measurements reveal a switching of the magnetization, with a horizontal intermediate magnetization, produced by a static horizontal field. (b) The magnetostrictive bending measured simultaneously. Vertical film magnetization causes the film to expand along its length. The magneto-elastic coupling induces a magnetostrictive compressive stress in the film that leads to a bending of the film–substrate composite.

bending of a flexible mounted substrate–film composite by induction voltages in pick-up coils [30], a voltage induced in a piezoelectric bimorph [31] or optical measurement of the maximum sample deflection in resonance [32]. Even UHV compatible microbalances have been realized for magnetometry of nanometre Fe films by measuring the forces on the film in an inhomogeneous field [33]. The magneto-elastic coupling that describes the effect of magnetostriction of ferromagnetic films that are not free, but

bonded to a substrate, can be investigated with the bending beam technique as well. Examples are given by the capacitive detection of the cantilever deflection [34] and by optical deflection techniques [35] that can be enhanced in sensitivity by lock-in techniques [36]. Whereas the experiments cited were all tailored towards a maximum sensitivity either for magnetometry or for magnetostriction, our simple set-up allows one to perform measurements on the magnetometry and magnetostriction of nanometre films in addition to *in situ* stress measurements. This combined use of the cantilever technique to measure the stress dependence of the magneto-elastic coupling in 100 nm Fe films was recently demonstrated by Koch [37].

The growth of 110 nm Fe on W(100) leads to easy axes of magnetization along the sample length and along the sample width. Thus, the Fe film can be magnetized along its length by the UHV magnet (2) of figure 2 in position (3). The external magnet is rotated to the polar position and the application of a magnetic field perpendicular to the sample surface leads to a bending of the crystal due to the induced torque, as shown in figure 7(a). The torque is proportional to the sample curvature $1/R$. Thus, from the slope of the curve position signal versus deflection field, the total magnetic moment of the Fe film can be calculated with a high relative accuracy, as indicated in figure 7(b) by measurements of two separate runs. A magnetic moment close to the bulk value of Fe (2.2 μ_{Bohr}) was obtained. Note that the geometry of the set-up requires sample magnetization along the sample length, with a deflection field oriented perpendicular to the surface, or vice versa.

Magneto-elastic coupling of the same Fe film was measured by the magnetostrictive bending of the film–substrate composite. To evaluate the bending due to magnetostriction it is essential to switch the magnetization between two well-defined states. As indicated in figure 8(a), transversal MOKE was employed to monitor the magnetization of the film along its length. A static horizontal field was produced by the external magnet, the vertical field was swept to switch the magnetization from downwards, to horizontal, to upwards, as indicated in figure 8(a). In addition to the MOKE signal, the bending of the crystal was monitored simultaneously, as shown in figure 8(b). The magnetization in the vertical direction induced a negative position signal that corresponded to an expansion of the Fe film upon magnetization. Thus, a magnetostriction signal was obtained that could be correlated to the respective magnetization states, measured *in situ* with MOKE. On following the procedure to convert curvature to magnetostriction outlined by Marcus [14], a magnetostriction constant $\lambda_{100} = 5 \times 10^{-6}$ resulted, which is only a quarter of the quoted value for bulk Fe [38]. Currently, Kerr-imaging studies to monitor the magnetization reversal of the whole sample are under way. A switching of the magnetization direction that is limited to only parts of the crystal would be a natural explanation for the small magnetostrictive signal. For decreasing film thicknesses the magnetostriction constant was found to be thickness dependent. A negative magnetostriction constant of -6.7×10^{-6} was measured for 3 nm Fe on W(100). This deviation of the magneto-elastic coupling from bulk behaviour suggests that *surface* magneto-elastic coupling is a more appropriate description of magneto-elasticity in ultrathin films [39].

7. Conclusions and outlook

The *in situ* combination of stress measurements with magneto-optical Kerr-effect measurements reveals experimental evidence for the intimate relation between the film stress and the magnetism. Stress-driven structural changes like the formation of a misfit distortion network for room-temperature growth of Fe on W(110) and the coalescence of Fe into 3D islands for high-temperature Stranski–Krastanov growth induce a high coercivity of the sesquilayer Fe film and an in-plane re-orientation of the easy axis of magnetization, respectively. The high sensitivity of the optical deflection technique for measuring stress allows a determination of magnetostrictive effects in nanometre ferromagnetic films. The magneto-elastic coupling in ultrathin films was found to be thickness dependent, in contrast to the respective bulk behaviour. The stress measurements indicated that, for sub-monolayer coverages, the concept of lattice mismatch does not describe the film stress adequately. It is rather the surface stress of the substrate–film composite that governs the sub-monolayer stress. The experimental results on stress and magneto-elastic coupling in the monolayer range cannot be adequately described by models based on bulk behaviour. A more appropriate description of epitaxial growth and magneto-elastic coupling that goes beyond the concepts of lattice mismatch is required in order to allow one to gain a deeper understanding of the relevant processes on an atomic scale.

Acknowledgment

The authors acknowledge intensive discussions with U Gradmann on the magnetism of Fe monolayers.

References

[1] Falicov L M, Pierce D T, Bader S D, Gronsky R, Hathaway K B, Hopster H J, Lambeth D N, Parkin S S P, Prinz G, Salamon M, Schuller I K and Victora R H 1990 *J. Mater. Res.* **5** 1299
[2] Howson M A 1994 *Contemp. Phys.* **35** 347
[3] Gradmann U 1993 *Handbook of Magnetic Materials* vol 7, ed K H J Buschow (Amsterdam: Elsevier) ch 1
[4] Bland J A C and Heinrich B (eds) 1994 *Ultrathin Magnetic Structures 1994* vol 1 and 2 (Berlin: Springer)
[5] Kolaczkiewicz J and Bauer E 1986 *Surf. Sci.* **175** 508
[6] Gradmann U and Waller G 1982 *Surf. Sci.* **116** 539
[7] Bethge H, Heuer D, Jensen Ch, Reshöft K and Köhler U 1995 *Surf. Sci.* **331–33** 878
[8] Kolaczkiewicz J and Bauer E 1984 *Surf. Sci.* **144** 495
[9] Schmidthals C, Enders A, Sander D and Kirschner J 1998 *Surf. Sci.* at press
Sander D, Schmidthals C, Enders A and Kirschner J 1998 *Phys. Rev.* B at press
[10] Marcus P M and Jona F 1995 *Phys. Rev.* B **51** 5263
[11] Stoney G G 1909 *Proc. R. Soc.* A **82** 172
Ibach H 1997 *Surf. Sci. Rep.* **237**
[12] Brantley W A 1972 *J. Appl. Phys.* **44** 534
[13] Marcus P M 1996 *Phys. Rev.* B **53** 7460
Marcus P M 1996 *Surf. Sci.* **366** 219
[14] Marcus P M 1997 *J. Magn. Magn. Mater.* **168** 18

[15] Weber M, Koch R and Rieder K H 1994 *Phys. Rev. Lett.* **73** 1166
Sander D and Ibach H 1991 *Phys. Rev.* B **43** 4263
[16] Schell-Sorokin A J and Tromp R M 1990 *Phys. Rev. Lett.* **64** 1039
Martinez R E, Augustyniak G A and Golovchenko J A 1990 *Phys. Rev. Lett.* **64** 1035
[17] Sander D, Enders A and Kirschner J 1995 *Rev. Sci. Instrum.* **66** 4734
[18] Sander D, Linke U and Ibach H 1992 *Surf. Sci.* **272** 318
[19] Weber M, Koch R and Rieder K H 1994 *Phys. Rev. Lett.* **73** 1166
[20] This number reflects the state of the art of capacitive techniques as employed by R Koch at the FU Berlin (private communication) and also of our optical deflection technique
[21] Bader S M 1991 *J. Magn. Magn. Mater.* **100** 440
[22] Sander D, Skomski R, Schmidthals C, Enders A and Kirschner J 1996 *Phys. Rev. Lett.* **77** 2566
Sander D, Schmidthals c, Enders A and Kirscher J 1998 *Phys. Rev* B at press
[23] Gradmann U, Liu G, Elmers H J and Przybylski M 1990 *Hyperfine Interactions* **57** 1845
[24] Reuter D, Gerth G and Kirschner J 1996 *Surface Diffusion: Atomistic and Collective Processes* ed M Tringides (New York: Plenum)
[25] Kneller E 1962 *Ferromagnetismus* (Berlin: Springer)
[26] Sander D, Enders A, Schmidthals C, Reuter D and Kirschner J 1998 *J. Magn. Magn. Mater.* at press
[27] Fritzsche H, Elmers H J and Gradmann U 1994 *J. Magn. Magn. Mater.* **135** 343
[28] Prinz G A, Rado G T and Krebs J J 1982 *J. Appl. Phys.* **53** 2087
[29] Gradmann U, Korecki J and Waller G 1986 *Appl. Phys.* A **39** 101
[30] Lewis R T 1976 *Rev. Sci. Instrum.* **47** 519
[31] Roos W, Hempel K A, Voigt C, Dederichs H and Schippan R 1980 *Rev. Sci. Instrum.* **51** 612
[32] Ziljstra H 1970 *Rev. Sci. Instrum.* **41** 1241
[33] Stünkel D 1963 *Z. Phys.* **176** 207
[34] Klokholm E 1976 *IEEE Trans. Magn.* **12** 819
[35] Betz J, du Trémolet de Lacheisserie E and Baczewski L T 1996 *Appl. Phys. Lett.* **68** 132
[36] Tam A C and Schroeder H 1989 *IEEE Trans. Magn.* **25** 2629
[37] Koch R, Weber M, Thürmer K and Rieder K H 1996 *J. Magn. Magn. Mater.* **159** L11
[38] Lee E W 1955 *Rep. Prog. Phys.* **18** 184
[39] Sun S W and O'Handley R C 1991 *Phys. Rev. Lett.* **66** 2798
Song O, Ballentine C and O'Handley R C 1994 *Appl. Phys. Lett.* **64** 2593